Capillary Interception of Floating Particles by Surface-Piercing Vegetation

Paolo Peruzzo,[1] Andrea Defina,[1] Heidi M. Nepf,[2] and Roman Stocker[2,*]

[1]*Dipartimento di Ingegneria Civile, Edile e Ambientale, University of Padova, Via Loredan 20, 35131 Padova, Italy*
[2]*Department of Civil and Environmental Engineering, MIT, Cambridge, Massachusetts 02139, USA*

Surface-piercing vegetation often captures particles that flow on the water surface, where surface tension forces contribute to capture. Yet the physics of capillary capture in flow has not been addressed. Here we model the capture of floating particles by surface-piercing collectors at moderately low Reynolds numbers (Re < 10). We find a trade-off between the capillary force, which increases with the collector diameter, and the relative size of the meniscus, which decreases with the collector diameter, resulting in an optimal collector diameter of $\sim 1 - 10$ mm that corresponds to the regime in which many aquatic plant species operate. For this diameter range the angular distribution of capture events is nearly uniform and capture can be orders of magnitude more efficient than direct interception, showing that capillary forces can be major contributors to the capture of seeds and particulate matter by organisms.

　　　　PACS numbers: 47.15.−x, 47.11.−j, 47.55.nb, 87.16.dp

The interception of particles by aquatic vegetation is a fundamental process in many aquatic ecosystems, with important implications for seed dispersal (hydrochory) [1,2] and organic matter retention [3,4]. For suspended particles, a primary mechanism for capture is direct interception [5], where particles transported by flow in the close vicinity of a vegetation element are captured by direct contact. However, this mechanism cannot fully describe the capture of floating particles, which is affected by the capillary forces associated with the free surface deformation induced by the collector and by the particles themselves [6].

Capillary attraction can cause motion and clustering of objects on the surface of a liquid, as in the Cheerios effect, the clustering of cereal floating on milk [7]. In aquatic environments, this results in the aggregation and capture by surface-piercing vegetation of floating seeds [8–10] and buoyant insect eggs, including those of the *Anopheles* mosquito [11]. Different parts of a plant can act as surface-piercing collectors, including stems (~ 10 mm), branches (~ 1 mm), thorns and hairs (~ 0.01–0.1 mm). Yet, despite results pointing at the importance of capillary capture in flowing fluid [8–10,12], no physically based framework currently exists for this process. Here, we study capillary capture in flow using the first physically based mathematical model, and focusing on the slow flowing conditions typical of many natural systems [13].

We consider small floating particles on the surface of flowing liquid and their capture by a vertical surface-piercing cylindrical collector [Fig. 1(a)], which models vegetation with long stems or branches, such as cord grass (*Spartina*), sedges (*Carex*), and reed (*Phragmites*). Our results apply to particles and collectors that have positive menisci angles, the most common case in

aquatic systems, but are straightforward to extend to particles and collectors that both have negative menisci angles [6]. We determine particle trajectories by integrating the Basset-Boussinesq-Oseen equation [14], modified to account for capillary forces [15]. In dimensionless form,
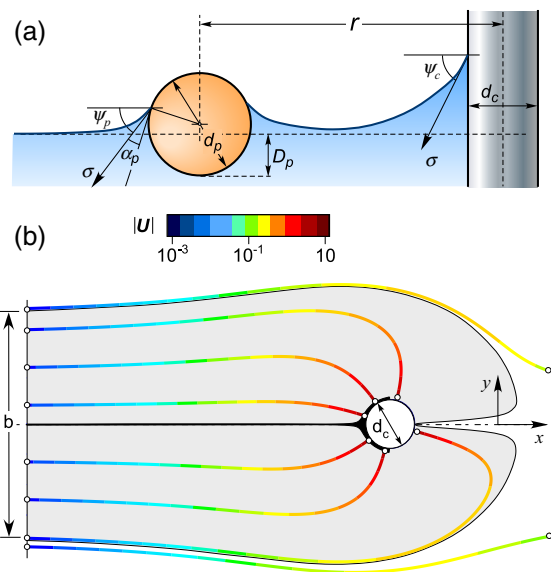

FIG. 1 (color online). Capillary capture in flow. (a) The meniscus between particle and collector attracts the particle towards the collector. (b) Trajectories of floating particles, showing the capture area (gray area). The black area is the capture area without capillary forces, i.e., by direct interception alone. Trajectories are color coded by the relative particle velocity |**U**| and the collector's center is at $x = 0$ (axes are shown displaced for clarity). Parameters were Re = 1, $d_c = 1.0$, $d_p = 0.1$, $\rho_p = 0.7$, $\psi_c = 80°$, $\alpha_p = 60°$.

$$(\rho_p + \beta)\frac{d\mathbf{u}_p}{dt}$$

$$= \frac{3C_D}{4d_p}\mathbf{U}|\mathbf{U}| + \xi\frac{6\sqrt{\nu/\pi}}{d_p}\int_0^t \frac{d\mathbf{U}/d\tau}{\sqrt{t-\tau}}d\tau + (1+\beta)\frac{d\mathbf{u}_f}{dt}$$

$$- \frac{3}{R^2\mathrm{We}}\sin\vartheta_p\sin\psi_p\sin\psi_c K_1(r)\hat{\mathbf{r}}, \qquad (1)$$

where all variables without tildes have been made dimensionless using the fluid density $\tilde{\rho}_f$, the incoming flow velocity $\tilde{u}_0$ (typically ranging from 1 to 100 mm/s in aquatic systems), and the capillary length $\tilde{\lambda} = (\tilde{\sigma}/\tilde{\rho}_f\tilde{g})^{1/2}$, which is the characteristic length scale of the meniscus, with $\tilde{\sigma}$ the surface tension. Here we focus on a water-air interface, hence $\tilde{\sigma} = 0.073$ N/m and $\tilde{\lambda} = 2.7$ mm. Subscripts p, c, and f denote variables referring to the particle, collector, and fluid, respectively, t is time, and r is the distance from the collector's center. Equation (1) expresses the balance of forces on a floating particle including (in this order, on the right-hand side) the drag force, Basset history force, added mass force, and capillary force. ρ_p is the dimensionless particle density, $\mathbf{U} = \mathbf{u}_f - \mathbf{u}_p$ is the difference between the fluid velocity $\mathbf{u}_f$ and the particle velocity $\mathbf{u}_p$, $R = d_p/d_c$ is the ratio between the particle diameter and the collector diameter, $\xi = A_p d_p/V_p$ and $\beta = D_p A_p/(3V_p)$ are shape factors, A_p and V_p are the particle's waterline area and volume, D_p is the particle's draft, $C_D = 24/(\mathrm{Re}R|\mathbf{U}|) + 6/(1 + \sqrt{\mathrm{Re}R|\mathbf{U}|}) + 0.4$ [16] is the drag coefficient, $\mathrm{Re} = \tilde{d}_c\tilde{u}_0/\tilde{\nu}$ is the Reynolds number, with $\tilde{\nu}$ the kinematic viscosity, and K_1 is the modified Bessel function of order 1. The Weber number, $\mathrm{We} = \tilde{\rho}_f\tilde{d}_c\tilde{u}_0^2/\tilde{\sigma}$, measures the relative magnitude of inertial force and capillary force, where the latter acts in the direction $\hat{\mathbf{r}}$ connecting the centers of the particle and the collector. ψ_p, ψ_c, and $\vartheta_p = \alpha_p + \psi_p$ are angles related to the menisci of the particle and the collector [Fig. 1(a)]. The meniscus angle ψ_p at the particle surface is determined from the vertical force balance for a floating hydrophilic sphere [17]. The validity of the linearized solution adopted for the capillary force in Eq. (1) is related to the values of these angles: when ψ_p and ψ_c are large, the capillary force is well estimated only for large distances between the particle and the collector [15].

We quantified capillary capture for a cylinder piercing the surface in a uniform incoming flow. We determined the flow with a finite element code (COMSOL MULTIPHYSICS) and integrated Eq. (1) using a backward Euler scheme for 1000 particles per run, initialized at different transverse (y) positions far upstream of the collector ($x = -20d_c$). We followed each particle until it was captured (i.e., it came within a particle radius of the collector) or left the domain ($x > 20d_c$). We thus quantified the capture width b [Fig. 1(b)], defined as the flow cross

section far upstream of the collector from which all particles are captured, and hence the capture efficiency $\eta = b/d_c$ [18]. Because we focus on water, the parameter $\mathrm{We}\,\mathrm{Bo}^{1/2}/\mathrm{Re}^2 = (\tilde{\mu}/\tilde{\sigma}^2)(\tilde{g}/(\tilde{\sigma}\tilde{\rho}_f))^{1/2} = 5\times10^{-6}$ is constant, where $\mathrm{Bo} = \tilde{\rho}\,\tilde{g}\,\tilde{d}_c^2/\tilde{\sigma}$ is the Bond number, which measures the relative importance of gravity and surface tension, and $\tilde{\mu}$ is the dynamic viscosity.

The capture area [shaded gray, Fig. 1(b)] reveals that, contrary to other capture mechanisms, capillary attraction triggers captures also on the back side of the collector [17]. Particles starting close to the center line are captured on the front of the collector, whereas particles starting farther from the center line contact the collector on its back side. Capillary interception is thus qualitatively different from direct interception, where capture occurs only on the front side of the collector. This is clearly revealed by a comparison of the capture area with (gray) and without capillary forces [black, Fig. 1(b)] [17], which shows that the capture area can be far greater when capillary interception is included. A quantification of the particle Reynolds number, $\mathrm{Re}_p = \tilde{d}_p\tilde{U}/\tilde{\nu}$, along the trajectories showed that in the majority of cases we are strictly within the range of validity of the Basset-Boussinesq-Oseen equation, i.e., $\mathrm{Re}_p < 1$ [19], and only in limited cases in the vicinity of the cylinder this value is slightly exceeded ($\mathrm{Re}_{p,\max} < 3$).

The total capture efficiency η can be several orders of magnitude larger than the capture efficiency by direct interception alone, η_D, in particular for large collector diameters ($d_c > 0.1$) (Fig. 2). For slow incoming flows, η reaches values above 10, indicating that capillary attraction allows the collector to capture particles from a distance much larger than its size. As the flow velocity (i.e., the Weber number) increases, η slowly decreases (Fig. 2), on account of the decreasing capillary capture, which is primarily controlled by the ratio of inertial to capillary forces. In contrast, the efficiency of capture by direct
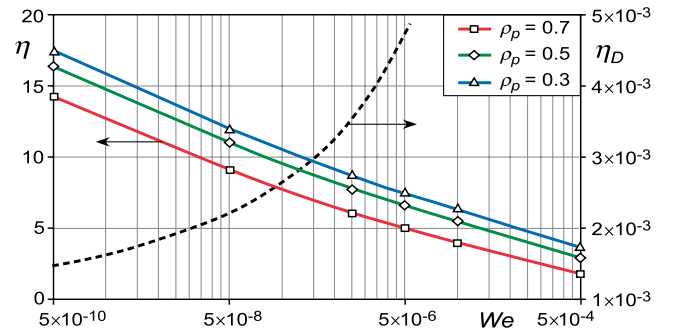

FIG. 2 (color online). Capillary capture can be considerably more efficient than direct interception. The total capture efficiency $\eta = \eta_C + \eta_D$ is shown as a function of the Weber number We for three particle densities ρ_p (solid lines). The dashed line is the efficiency of capture by direct interception alone, η_D [23]. Note the different scale for η and η_D. Parameters were $d_c = 1.0$, $d_p = 0.1$, $\mathrm{Bo} = 1$, $\alpha_p = 60°$, $\psi_c = 80°$.
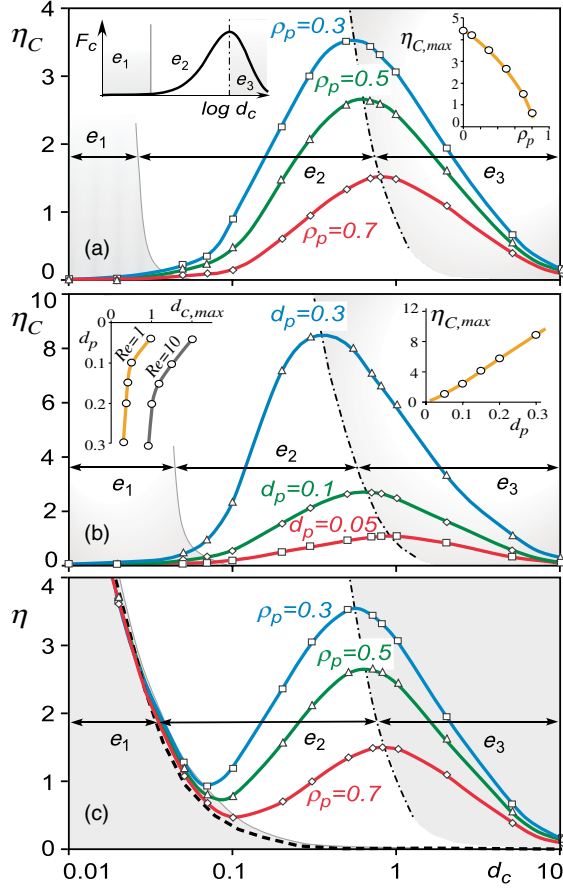
FIG. 3 (color online). Capillary capture efficiency η_C as a function of collector diameter d_c for (a) three particle densities, ρ_p, and $d_p = 0.1$; and (b) three particle diameters d_p and $\rho_p = 0.5$. Parameters were Re = 1, $\psi_c = 5°$, and $\alpha_p = 60°$. (c) Total capture efficiency $\eta = \eta_C + \eta_D$ for the same case as in panel (a). The thick dashed line shows the efficiency of direct interception η_D for $\rho_p = 0.5$ (solutions for $\rho_p = 0.3$ or 0.7 differ by <1.5%). In all panels, the thin black dash-dotted line is the envelope of the capture efficiency peaks, and right insets show the maximum capillary capture efficiency $\eta_{C,\max}$. The left inset in (a) shows the functional dependence of the capillary force F_C on the collector diameter d_c [Eq. (2)]. The left inset in (b) shows the position of the maxima for Re = 1 and Re = 10.

interception, η_D, increases with flow velocity, because direct interception depends on how close a streamline comes to the collector and inertia compresses streamlines towards the collector.

To gain insight into the mechanisms governing capillary capture in flow, we quantified the capillary capture efficiency, $\eta_C = \eta - \eta_D$, by varying the particle density ρ_p [Fig. 3(a)], or the particle size d_p [Fig. 3(b)], at a given Reynolds number. Capillary capture efficiency is greater for lighter particles [Fig. 3(a)]. This results from the competition between capillary forces, which attract the particle to the collector and favor capture, and inertial forces from the flow, which sweep the particle past the collector, inhibiting capture. Lighter particles have lower inertia

and experience stronger attraction, because they rise further above the water surface, and both effects enhance capture.

The increase of η_C with particle size d_p [Fig. 3(b)] is somewhat less intuitive, given that larger particles have greater inertia. However, larger particles also induce a steeper meniscus angle ψ_p [17], and thus a larger capillary force [Eq. (1)]. This effect prevails over the increase in inertia and, thus, larger particles are captured more efficiently than smaller ones at least up to $d_p = 3 - 10$, above which ψ_p no longer increases with d_p [17]. The same behavior is found by increasing the cylinder meniscus slope ψ_c [17].

The capillary capture efficiency η_C displays a clear maximum as a function of the collector size d_c [Figs. 3(a) and 3(b)]. This maximum can be understood by an analysis of the dependence of the capillary force F_C [last term in Eq. (1)], on the collector diameter d_c [17]

$$F_C \sim d_c^3 K_1(\varepsilon d_c), \qquad (2)$$

with ε a constant. This functional dependence has a bell shape [Fig. 3(a), left inset], which accounts for the maximum in η_C. In contrast the direct interception efficiency η_D decreases monotonically with increasing d_c [heavy dashed line in Fig. 3(c)]. Accordingly, the total capture efficiency $\eta = \eta_C + \eta_D$ displays three different regimes (e_1, e_2, e_3) as a function of the collector size d_c [Fig. 3(c)]: for $d_c \lesssim 0.1$, η decreases with increasing d_c; for d_c up to ~1, η increases with d_c; and for $d_c \gtrsim 1$, η again decreases with increasing d_c. These trends reflect the dynamics of the three regimes. For very small collectors ($d_c \lesssim 0.1$), the capillary force F_C is small ($\sim d_c^3$), whereas direct interception is important [dashed line in Fig. 3(c), corresponding to $\eta_D \approx 1 + R > 1$ in this regime; [20]], because particles follow nearly straight streamlines and their speed is relatively large (since Re = const). Thus, total capture is dominated by direct interception [17], whose efficiency decreases with increasing d_c. For intermediate collectors (d_c up to ~1), F_C increases considerably ($\sim d_c^3$), whereas η_D continues to decrease [Fig. 3(c)], and thus capture is dominated by capillary capture [17]. Finally, for large collectors ($d_c \gtrsim 1.0$), F_C decreases with increasing d_c because the collector is too large to considerably deform the free surface relative to its own size [as reflected in the strong decrease in K_1 in Eq. (2)]. However, η_D decreases even more strongly [Fig. 3(c)] and thus capture is again dominated by capillary capture [17], which decreases with increasing d_c.

The effect of capillary forces can be understood in more detail by considering the angular distribution of capture events along the perimeter of the collector (Fig. 4). For very small collectors, the dominance of direct interception is confirmed by the concentration of capture events along the front of the collector [Fig. 4(c)]. The variance σ_θ of the angular distribution of captured particles, normalized by
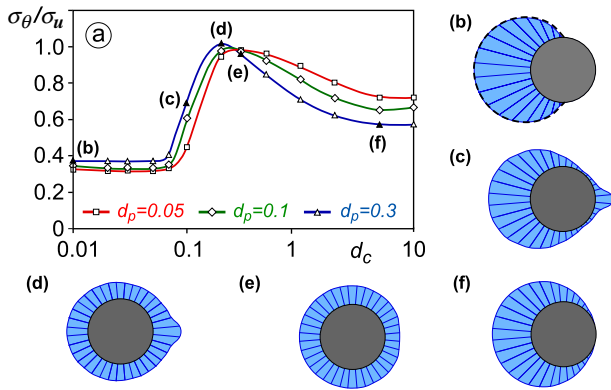
FIG. 4 (color online). The distribution of capture events around the perimeter of the collector. (a) The variance σ_θ of the angular distribution of captured particles, normalized by the variance $\sigma_u = \pi/\sqrt{3}$ of a uniform distribution, as a function of the collector diameter d_c for three particle diameters, for Re $= 1$, $\rho_p = 0.5$, $\psi_c = 5°$, and $\alpha_p = 60°$. (b)–(f) The angular distribution of capture events for different collector diameters [see labels in (a)] and $d_p = 0.3$. The dashed line in (b) shows the angular distribution of captures by direct interception. Flow is from left to right.

the variance $\sigma_u = \pi/\sqrt{3}$ of a uniform distribution, provides a measure of the departure from a uniform capture. For direct interception, $\sigma_\theta/\sigma_u \approx 0.37$. As the collector diameter increases, capture occurs also on its back side, owing to capillary capture, making the capture distribution more uniform [Fig. 4(c)]. The maximum capture efficiency corresponds to a nearly uniform capture distribution. When η_C is maximum ($d_c = 0.3$–0.8; Fig. 3), $\sigma_\theta/\sigma_u = 0.8$–$1.0$. The most uniform capture distribution [$\sigma_\theta/\sigma_u = 0.96$–$1.01$, Fig. 4(b)] occurs for $d_c = 0.2$–0.3, which falls just outside the range yielding maximum capture efficiency. It is worth noting that values of $\sigma_\theta/\sigma_u > 1.0$ imply particle distributions skewed towards the back of the cylinder. By favoring capture on the back side of the collector, capture by capillarity further ensures that many particles are sheltered from subsequent dislodging by collision with other particles or drag forces due to increased flow. Finally, we note that an increase in Reynolds number shifts the optimum toward somewhat larger collector diameters: for example, the optimal diameter is $d_c = 0.3$–0.8 for Re $= 1$ and $d_c = 1.0$–2.0 for Re $= 10$ [Fig. 3(b), left inset].

In summary, the capture of floating particles from a flowing stream by means of capillary forces is important *vis-á-vis* direct interception ($\eta_C > \eta_D$) for dimensionless collector diameters ranging from 0.2 to 10, or 0.5 to 27 mm in water. Because many aquatic plants have stems or appendages that fall within this size range, we expect that plants widely use this passive mechanism to collect particles from flowing water. Whether collector size or particle size have evolved to favor capillary capture remains an open question. Production of seeds of the

appropriate size may represent a strategy to favor capillary capture, a hypothesis supported by the observation that seed size often falls in the predicted optimal range (e.g., *Salicornia* with $\tilde{d}_p \sim 1$ mm and *Spergularia media* with $\tilde{d}_p \sim 0.8$ mm; i.e., $d_p < 1$ in dimensionless size) [21].

The extent to which results can be directly applied to natural systems depends on the additional complexities of the specific system. Stem density is rarely a problem, because the assumption of dilute stem concentrations applies to most aquatic ecosystems [12], with the notable exception of the leaves of some plants (e.g., *Spartina maritima*), which can be very close to each other and capture particles by forming netlike structures [9]. Small deviations in the shape of collector or particles will not change capture significantly; however, our model does not apply to species with extensive leafy foliage, as the elongated cross section of leaves causes a spatially variable meniscus elevation [22]. The model also does not capture the case of concentrated particle fields, for example, when particles interact and cluster. Ultimately, these results and the added complexities expected in natural systems call for careful experiments, to obtain a deeper understanding of this elegant capture mechanism, its fitness advantages for aquatic vegetation, and its potential use by a broader range of aquatic organisms.

*Corresponding author.
romans@mit.edu

[1] T. Riis and K. Sand-Jensen, Freshwater Biol. **51**, 274 (2006).
[2] M. Merrit and E. E. Wohl, Ecol. Appl. **12**, 1071 (2002).
[3] C. Nilsson, R. L. Brown, R. Jansson, and D. M. Merritt, Biol. Rev. Camb. Philos. Soc. **85**, 837 (2010).
[4] M. Harvey, E. Bourget, and R. G. Ingram, Limnol. Oceanogr. **40**, 94 (1995).
[5] D. I. Rubenstein and M. A. R. Koehl, Am. Nat. **111**, 981 (1977).
[6] P. A. Kralchevsky and N. D. Denkov, Curr. Opin. Colloid Interface Sci. **6**, 383 (2001).
[7] D. Vella and L. Mahadeven, Am. J. Phys. **73**, 817 (2005).
[8] S. Chambert and C. S. James, River Res. Appl. **25**, 48 (2009).
[9] A. Defina and P. Peruzzo, Water Resour. Res. **46** (2010).
[10] A. Defina and P. Peruzzo, Water Resour. Res. **48** (2012).
[11] L. V. Knutson and J. C. Vala, in *Biology of Snail-Killing Sciomyzidae Flies* (Cambridge University Press, Cambridge, 2011), pp. 161–170.
[12] P. Peruzzo, A. Defina, and H. M. Nepf, Water Resour. Res. **48** (2012).
[13] R. L. Schneider and R. R. Sharitz, Ecology **69**, 1055 (1988).
[14] S. Umeda and W. J. Yang, Exp. Fluids **12**, 106 (1991).

[15] C. D. Dushkin, P. A. Kralchevsky, V. N. Paunov, H. Yoshimura, and K. Nagayama, Langmuir **12**, 641 (1996).

[16] F. M. White, in *Viscous Fluid Flow*, edited by L. Beamesderfer and J. M. Morriss (McGraw-Hill, New York, 1991), 2nd ed., pp. 181–184.

[17] See Supplemental Material at http://link.aps.org/supplemental/10.1103/PhysRevLett.111.164501 for a short description of the equations, a movie, and figures.

[18] M. R. Palmer, H. M. Nepf, and T. J. R. Pettersson, Limnol. Oceanogr. **49**, 76 (2004).

[19] S. I. Green, in *Fluid Vortices: Fluid Mechanics and Its Applications* (Springer, Dodrecht, 1995), Vol. 30, p. 831.

[20] N. E. L. Haugen and S. Kragset, J. Fluid Mech. **661**, 239 (2010).

[21] E. R. Chang, R. M. Veeneklaas, R. Buitenwerf, J. P. Bakker, and T. J. Bouma, Funct. Ecol. **22**, 720 (2008).

[22] C. Pozrikidis, IMA J. Appl. Math. Mech. **75**, 418 (2010).

[23] I. Langmuir, Office of Scientific Research and Development Report No. 865, 1942.